Journal of Molecular and Cellular Cardiology 114 (2018) 10–19

Contents lists available at ScienceDirect

Journal of Molecular and Cellular Cardiology

journal homepage: www.elsevier.com/locate/yjmcc

Original article

Sodium channel current loss of function in induced pluripotent stem cell-derived cardiomyocytes from a Brugada syndrome patient

Elisabet Selga[a,b,c,1], Franziska Sendfeld[d,e,1], Rebecca Martinez-Moreno[a,b,c], Claire N. Medine[d,e], Olga Tura-Ceide[f,g], Sir Ian Wilmut[d], Guillermo J. Pérez[a,b,c], Fabiana S. Scornik[a,b,c,2], Ramon Brugada[a,b,c,h,2], Nicholas L. Mills[e,*,2]

[a] Cardiovascular Genetics Centre, Department of Medical Sciences, University of Girona, Girona, Spain
[b] Institut d'Investigació Biomèdica de Girona (IDIBGI), Girona, Spain
[c] Centro de Investigación Biomédica en Red de Enfermedades Cardiovasculares (CIBERCV), Spain
[d] Scottish Centre for Regenerative Medicine, University of Edinburgh, United Kingdom
[e] BHF/University Centre for Cardiovascular Sciences, University of Edinburgh, United Kingdom
[f] Department of Pulmonary Medicine, Hospital Clinic-Institut d'Investigacions Biomèdiques August Pi i Sunyer (IDIBAPS), University of Barcelona, Barcelona, Spain
[g] Centro de Investigación Biomédica en Red de Enfermedades Respiratorias, University of Barcelona, Spain
[h] Hospital Josep Trueta, Girona, Spain

ARTICLE INFO

Keywords:
Brugada syndrome
Pluripotent stem cells
Cardiomyocytes
Electrophysiology
Sodium current

ABSTRACT

Brugada syndrome predisposes to sudden death due to disruption of normal cardiac ion channel function, yet our understanding of the underlying cellular mechanisms is incomplete. Commonly used heterologous expression models lack many characteristics of native cardiomyocytes and, in particular, the individual genetic background of a patient. Patient-specific induced pluripotent stem (iPS) cell-derived cardiomyocytes (iPS-CM) may uncover cellular phenotypical characteristics not observed in heterologous models. Our objective was to determine the properties of the sodium current in iPS-CM with a mutation in *SCN5A* associated with Brugada syndrome.

Dermal fibroblasts from a Brugada syndrome patient with a mutation in *SCN5A* (c.1100G > A, leading to $Na_v1.5$_p.R367H) were reprogrammed to iPS cells. Clones were characterized and differentiated to form beating clusters and sheets. Patient and control iPS-CM were structurally indistinguishable. Sodium current properties of patient and control iPS-CM were compared. These results were contrasted with those obtained in tsA201 cells heterologously expressing sodium channels with the same mutation.

Patient-derived iPS-CM showed a 33.1–45.5% reduction in I_{Na} density, a shift in both activation and inactivation voltage-dependence curves, and faster recovery from inactivation. Co-expression of wild-type and mutant channels in tsA201 cells did not compromise channel trafficking to the membrane, but resulted in a reduction of 49.8% in sodium current density without affecting any other parameters.

Cardiomyocytes derived from iPS cells from a Brugada syndrome patient with a mutation in *SCN5A* recapitulate the loss of function of sodium channel current associated with this syndrome; including pro-arrhythmic changes in channel function not detected using conventional heterologous expression systems.

1. Introduction

Brugada syndrome is an autosomal dominant hereditary condition that is responsible for 20% of sudden cardiac deaths of patients with structurally normal hearts [1]. It is characterized by an abnormal electrocardiogram with ST-segment elevation in the right precordial leads V_1 to V_3 and right bundle-branch block frequently leading to ventricular fibrillation [2]. Patients often present symptoms of

Abbreviations: AFP, alpha-fetoprotein; CPVT, catecholaminergic polymorphic ventricular tachycardia; cTnI, cardiac troponin I; cTnT, cardiac troponin T; EB, embryoid body; HEK, human embryonic kidney cells; iPS, induced pluripotent stem cells; iPS-CM, iPS cell-derived cardiomyocytes; LQT, long QT syndrome; I_{Na}, sodium current; SNP, single nucleotide polymorphism; TEM, transmission electron microscopy; tsA201 cells, immortalized HEK293 cells

* Corresponding author at: BHF Centre for Cardiovascular Sciences, SU.226 Chancellor's Building, Royal Infirmary of Edinburgh, 49 Little France Crescent, Edinburgh EH16 4SU, United Kingdom.
E-mail address: nick.mills@ed.ac.uk (N.L. Mills).
[1] These authors contributed equally to this work.
[2] These authors contributed equally as corresponding authors.

http://dx.doi.org/10.1016/j.yjmcc.2017.10.002
Received 8 September 2016; Received in revised form 15 September 2017; Accepted 4 October 2017
Available online 09 October 2017

ventricular tachycardia, bradycardia, and atrial ventricular node conduction disorder, and more males than females are diagnosed with Brugada syndrome. To date, the implantation of a cardioverter defibrillator is the only proven effective treatment of the disease [3,4].

Whilst Brugada syndrome has been associated with mutations in 23 genes [5], the majority of these disease-related mutations have been found in *SCN5A* [6]. This gene encodes the alpha-subunit of the cardiac sodium channel ($Na_v1.5$) which is responsible for the sodium inward current (I_{Na}). Heterologous expression of recombinant $Na_v1.5$ channels in conventional cellular systems has provided invaluable insight into the molecular and electrophysiological basis of Brugada syndrome. Still, the main limitation of this approach is that the cells typically used (i.e., HEK293 cells, *Xenopus* oocytes) deviate considerably from human cardiomyocytes in many relevant aspects. These cells do not reflect the modulatory effects of accessory channel subunits or the influence of potential compensatory pathways, both of which could take place in native cardiomyocytes. Thus, studies of mutant channels using such expression systems might be missing important characteristics of native cardiomyocytes relevant to pathophysiology.

The differentiation of induced pluripotent stem (iPS) cells from patients with cardiac diseases into cardiomyocytes (iPS-CM) provides a cell model highly homologous to native human cardiomyocytes. The use of these surrogate cells allows investigators to study mutant ion channels in their native patient-specific cell environment. This includes all their regulatory proteins, and importantly, a physiologically controlled level of protein expression. To date, several cardiac channelopathies including long QT syndrome (LQT), catecholaminergic polymorphic ventricular tachycardia and Timothy syndrome have been modeled using the iPS cell approach [7]. Likewise, Davis et al. used iPS-CM to model an overlap LQT/Brugada syndrome [8]. Recently, BrS was modeled using patient-specific iPS-CM [9]. However, to date no reports exist that provide a complete characterization of the sodium current properties in Brugada syndrome patient-specific iPS-CM.

We generated iPS-CM from a patient diagnosed with Brugada Syndrome who carries a heterozygous missense mutation in *SCN5A* (c.1100G > A, leading to $Na_v1.5$_p.R367H). This mutation had been previously found in Brugada Syndrome patients [10,11]. Moreover, recombinant channels with this mutation were previously studied in homozygosis in both HEK293 cells and *Xenopus* oocytes [10–14]. These studies showed a total loss of function of the sodium current. Thus, we expected that, in iPS-CM, the presence of the $Na_v1.5$_p.R367H mutation in heterozygosis would cause a decrease near 50% of the total current due to the expression of non-functional channels translated from the mutant allele. To assess this assumption, we analyzed and compared sodium current properties of iPS-CM derived from the patient and from a healthy individual without this mutation.

2. Materials and methods

Detailed experimental procedures are available in the Online Data Supplement.

2.1. Isolation and reprogramming of fibroblasts to induced pluripotent stem (iPS) cells

This study was approved by the South East Scotland Research Ethics Committee REC reference 11-SS-0095 and written informed consent was obtained from the two subjects included in the study. Dermal biopsies were dissected into 1 mm^3 pieces, which were transferred to culture plastic, covered with a glass coverslip and cultured for 2 weeks before harvest. 5×10^5 fibroblasts were reprogrammed with the Addgene episomal vectors pCXLE-hOCT3/4-shp53-F (encoding for Oct4 and shp53, Addgene plasmid # 27077), pCXLE-hSK (Sox2 and Klf, Addgene plasmid # 27078) and pCXLE-hUL (LMyc and Lin28, Addgene plasmid # 27080). Reprogrammed fibroblasts were replated onto 0.1% gelatin and medium was changed to stem cell selection medium (TeSR-E8, STEMCELL Technologies SARL, Grenoble, France) 7 days post electroporation. Colonies appeared 15–20 days later. Individual clones were picked into Matrigel (BD Biosciences, Franklin Lakes, NJ, USA) coated tissue culture plates and maintained in TeSR-E8.

2.2. Sequencing

For all iPS cell lines, the whole coding region of *SCN5A* was amplified (Verities PCR, Applied Biosystems, Austin, TX, USA), the PCR products were purified (ExoSAP-IT, Affymetrix, Inc. USB® Products, Cleveland, OH, USA) and they were directly sequenced in both directions (Big Dye Terminator v3.1 cycle sequencing kit and 3130XL Genetic Analyzer, both from Applied Biosystems). DNA sequences obtained were compared with *SCN5A* reference sequence NM_198056.2 using SeqScape v2.6 (Applied Biosystems).

2.3. Real-time quantitative reverse transcription PCR (qPCR)

RNA extraction and cDNA synthesis were carried out according to manufacturer's specifications (Cambio, Cambridge, UK and Applied Biosystems-Thermo Fisher Scientific). qPCR reactions were set up using the GoTaq qPCR Master Mix kit (Promega, Madison, WI, USA), and included a reference dye. The samples were analyzed in biological triplicates using the primers listed in Supplemental Table 2 and run in a Rotor-Gene 6000 (Corbett Life Science-Qiagen, Manchester, UK). Expression levels were determined by the ΔΔCt method.

2.4. Flow cytometry

Undifferentiated iPS cells were double stained with fluorochrome-conjugated antibodies against SSEA-3 (Alexa Fluor 488 conjugate, BioLegend, San Diego, CA, USA) and SSEA-4 (Phycoerythrin conjugate, BD Biosciences) for 30 min at room temperature. Samples were run on a FACS Fortessa Flow Cytometry System acquiring a minimum of 10,000 events. Data was analyzed using FlowJo software (Treestar, Inc., San Carlos, CA, USA).

2.5. Single nucleotide polymorphism (SNP) analysis

Genomic DNA was isolated from undifferentiated iPS cells using the MasterPure™ Complete DNA & RNA Purification Kit (Cambio). Single nucleotide polymorphism (SNP) analysis was performed by AROS Applied Biotechnology A/S (Aarhus, Denmark) using the Illumina CytoSNP-12 array. Data was visualized and analyzed using the GenomeStudio V2011.1 software.

2.6. Differentiation

Embryoid bodies (EBs) were formed from confluent undifferentiated iPS cell colonies. Collagenase treatment and mechanical disruption resulted in roughly evenly sized clumps that were cultured in suspension on non-treated tissue culture dishes in serum-supplemented medium for 7 days at 37 °C and 5% CO_2. After a further 10 days on 0.1% gelatin coated tissue culture dishes, EBs were fixed and stained for the 3 germ layers.

For guided cardiac differentiation, two different protocols were used. First, a modified version of a published protocol [15] was implemented. In short, EBs were formed in supplemented Knock-out Dulbecco's Modified Eagle Medium, and cultured for 4 days in suspension and a further 10 days on 0.1% gelatin. Beating bodies started to emerge around day 8 after EB formation. Beating bodies were disaggregated using a previously published protocol [16,17].

The second protocol used was monolayer-based [18]. Briefly, iPS cells were allowed to grow to 85–90% confluence. Then, culture media was changed to differentiation medium containing CHIR99021 (Day 0). Twenty-four hours later, media was changed to differentiation medium

with heparin. From day 2 to day 5 the media contained both heparin and IWP2, and was renewed daily. At day 6, media was changed to differentiation medium with heparin only. The day after, the differentiation medium contained heparin and insulin. From day 8 onwards, cells were fed differentiation medium with insulin, and media was renewed every 2 days. iPS-CM started beating around day 8–10. iPS-CM monolayers were disaggregated with 0.25% trypsin-EDTA.

2.7. Immunocytochemistry

Undifferentiated cells were fixed in 4% paraformaldehyde for 10 min, permeabilized with 0.1% Triton X-100, blocked in 3% horse serum and stained for Nanog (R & D Systems, Abingdon, UK), Oct3/4 and Tra-1-60 (both from SantaCruz Biotechnology, Dallas, TX, USA). EBs differentiated to the three germ layers were fixed in cold methanol, permeabilized and blocked with 10% goat serum and stained for α-fetoprotein, β-tubulin III (both from Sigma-Aldrich, St. Louis, MO, USA) and Muscle actin (Dako, Glostrup, Denmark). Disaggregated beating bodies were fixed in 4% paraformaldehyde, permeabilized with 0.5% Triton X-100, blocked in 3% goat serum and stained for cardiac troponin T, cardiac troponin I, and alpha actinin (all from Abcam, Cambridge, UK). Appropriate secondary antibodies were used and cells were counterstained and mounted with ProLong Gold Antifade Reagent with DAPI.

2.8. Transmission electron microscopy (TEM)

Beating bodies were fixed in 2.5% glutaraldehyde in 4% PFA, washed with 0.1 mol/L Phosphate buffer, post-fixed in 1% Osmium Tetroxide in 0.1 mol/L Phosphate buffer, then washed with 0.1 mol/L Phosphate buffer. Samples were dehydrated in 50%, 70%, 90% and 100% ethanol, then in propylene oxide, and embedded in Araldite resin. Sections, 1 μm thick, were cut on a Reichert OMU4 ultramicrotome, stained with Toluidine Blue, and viewed in a light microscope to select suitable areas for investigation. Ultrathin sections, 60 nm thick, were cut from selected areas, stained in Uranyl Acetate and Lead Citrate then viewed in a Philips CM120 Transmission electron microscope. Images were taken on a Gatan Orius CCD camera.

2.9. Sodium current recordings in iPS-CM

Beating bodies and monolayers were disaggregated and plated onto 1% gelatin. Whole cell sodium currents were measured at room temperature either using the perforated patch-clamp technique 24–48 h after disaggregation (for beating bodies) or using the whole cell technique 24-96 h after disaggregation (for monolayers). Voltage clamp experiments were controlled and analyzed with an Axopatch 200B amplifier and pClamp 10.2/Digidata 1440A acquisition system (Molecular Devices, Sunnyvale, CA, USA) and OriginPro8 software (OriginLab Corporation, Northampton, MA, USA). Data were filtered at 5 kHz and sampled at 5–20 kHz. Activation curve data were fitted to a Boltzmann equation, of the form $g = g_{max} / (1 + \exp(V_{1/2} - V_m) / k)$, where g is the conductance, g_{max} the maximum conductance, V_m is the membrane potential, $V_{1/2}$ is the voltage at which half of the channels are activated and k is the slope factor. Steady-state inactivation values were fitted to a Boltzmann equation of the form $I = I_{max}/(1 + \exp(V_{1/2} - V_m)/k)$, where I is the peak current amplitude, I_{max} the maximum peak current amplitude, V_m is the membrane potential, $V_{1/2}$ is the voltage at which half of the channels are inactivated, and k is the slope factor. The sodium current decay after the peak I_{Na} was fitted with a monoexponential function between −40 and −25 mV, and a bi-exponential function between −20 and 20 mV, from where τ fast and τ slow were obtained. Both the slow inactivation and the recovery from inactivation data were fitted to mono-exponential functions, to obtain their respective time constants.

2.10. Sodium current recordings in tsA201 cells

2.10.1. Site-directed mutagenesis

*SCN5A*_c.1100G > A was introduced in the wild-type (WT) human *SCN5A* cDNA cloned in pcDNA3.1 using the QuikChange Site-Directed Mutagenesis system (Stratagene, La Jolla, CA, USA). The resultant construct was directly sequenced to verify the presence of the desired mutation and the absence of additional variations.

2.10.2. Cell culture and transfection

tsA201 cells were maintained as described previously [19] and transiently transfected with the vectors encoding for *SCN5A* ($Na_v1.5$_WT only, $Na_v1.5$_R367H only, or both WT and R367H vectors), using Lipofectamine 2000 (Life Technologies).

2.10.3. Electrophysiological studies

Sodium currents were measured at room temperature using the standard whole cell patch-clamp technique [20] 48 h after transfection. Voltage clamp experiments were controlled and analyzed as described for iPS-CM.

2.11. Cell surface protein biotinylation in tsA201 cells

Cells were plated and transfected as above and membrane proteins were biotinylated and isolated as previously described [19]. Proteins were resolved in 4% SDS-PAGE gels and transferred to PVDF membranes. Membranes were probed with an anti-human $Na_v1.5$ antibody (Alomone Labs, Jerusalem, Israel) and a secondary horseradish peroxidase-conjugated antibody (Thermo Scientific, Rockford, IL, USA). Signals were detected with the SuperSignal West Femto Chemiluminiscent substrate (Pierce, Thermo Scientific). A mouse antibody against Na^+/K^+ ATPase (Abcam) was used as biotinylation control. Expression of $Na_v1.5$ was quantified using ImageJ software (National Institute of Health, NIH).

2.12. Statistical analysis

Results are presented as mean ± standard error. Statistical comparisons were performed using an unpaired Student's *t*-test or two-way ANOVA with Bonferroni or Dunnett's post-test for multiple comparisons as appropriate. Statistical significance was defined where $p < 0.05$.

3. Results

3.1. Generation of iPS cell lines

A male Caucasian patient, aged 69, clinically diagnosed with Brugada syndrome was identified through the Familial Arrhythmia Network for Scotland. He presented with classical ST-segment elevation in the electrocardiogram (Fig. 1) and was found to have a missense mutation in *SCN5A* (c.1100G > A, leading to $Na_v1.5$_p.R367H) in heterozygosis. This mutation is located in the pore region of the first domain of $Na_v1.5$. We obtained and processed in parallel skin biopsies from this patient and an age and sex-matched healthy volunteer. Emerging fibroblasts were reprogrammed using episomal vectors and, under stem cell selection conditions, possible iPS cell colonies, assessed based on morphology, appeared after around 20 days. Colonies were

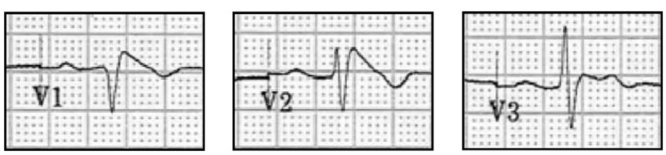

Fig. 1. Clinical manifestation of Brugada syndrome. Partial electrocardiogram of the proband showing the ST segment elevation characteristic of Brugada syndrome.

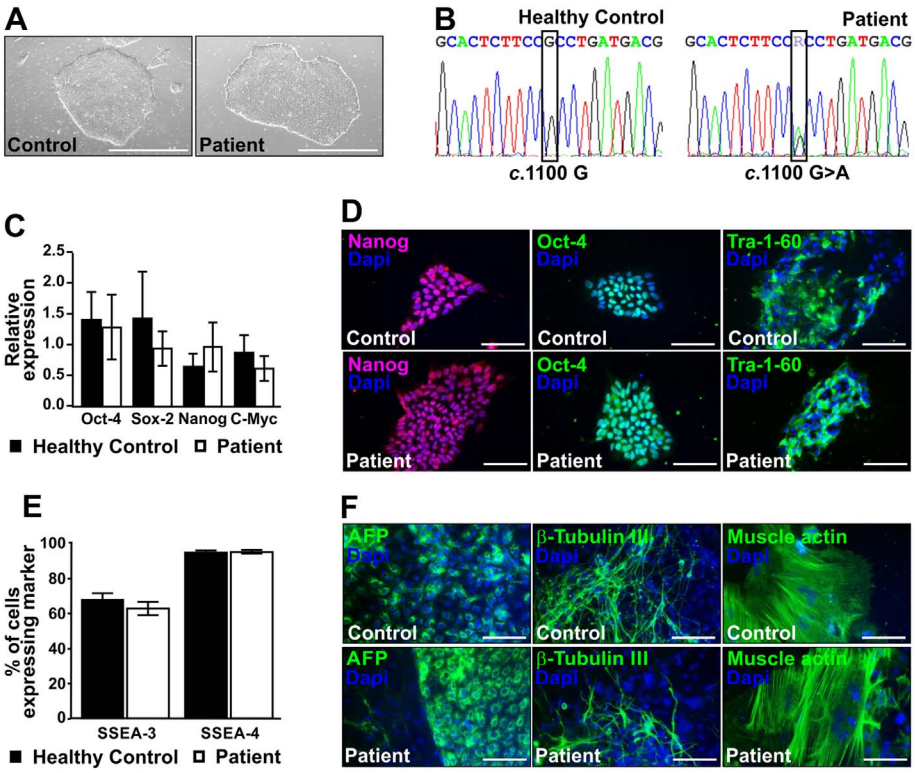

Fig. 2. Control and patient-specific iPS cell lines express pluripotency markers. (A) Representative light microscopy images of healthy control (left) and patient (right) newly derived induced pluripotent stem (iPS) cells in feeder-free culture. Scale bars represent 1000 μm. (B) The missense mutation *SCN5A*_c.1100G > A was identified in genomic DNA isolated from patient (right) but not healthy control derived iPS cells (left). (C) The relative expression of pluripotency transcription factors Oct-4, Sox2, Nanog and c-Myc in undifferentiated cells is shown as mean values of biological triplicates ± SEM. (D) Representative merged images of undifferentiated iPS cells showing positive staining for pluripotency markers Nanog, Oct-4 and Tra-1-60 for both control (upper panels) and patient (lower panels) iPS cells. Nuclei were counterstained with DAPI (blue). Scale bars represent 100 μm. (E) The percentage of SSEA-3 and SSEA-4 positive cells in undifferentiated iPS cell cultures is given as the mean of at least three independent wells ± SEM (F) Embryoid bodies (EBs) were formed from undifferentiated iPS cells and differentiated in suspension for 7 days and for an additional 10 days adhered to plates. Control (upper panels) and patient (lower panels) derived EBs showed positive staining for all three germ layers endoderm (AFP), ectoderm (β-tubulin III) and mesoderm (muscle actin). Nuclei were counterstained with DAPI (blue). Scale bars represent 100 μm.

treated as individual clones, manually picked and expanded in feeder-free conditions to give rise to independent cell lines. Each cell line grew in flat densely packed colonies with cells exhibiting the high nucleus to cytoplasm ratio typical for embryonic stem cells (Fig. 2A). Sequencing of the whole coding region of *SCN5A* in genomic DNA samples of all cell lines confirmed the presence of *SCN5A*_c.1100G > A in the patient lines, and its absence in the control lines (Fig. 2B). We also identified 3 synonymous SNVs (rs6599230, rs7430407 and rs1805126) that were present in all lines.

3.2. Characterization of patient and control iPS cell lines

To verify that the iPS cell lines expressed pluripotency markers, RNA was extracted from undifferentiated cultures, purified and reverse transcribed for each sample in biological triplicate and assessed for the relative expression of *POU5F1* (the gene encoding Oct-4), *Sox2*, *Nanog* and *c-Myc* (Fig. 2C). One-way ANOVA showed no differences in expression of the tested pluripotency transcription factors between patient and control iPS cell lines. We also fixed and stained undifferentiated pluripotent stem cells for the pluripotency markers Nanog, Oct-4 and Tra-1-60. As expected, both patient and control cell lines showed nuclear Nanog and Oct-4 staining, and cell surface staining for Tra-1-60 (Fig. 2D). Differentiated cells surrounding the colonies did not stain for pluripotency markers but were visible as DAPI stained nuclei. Using flow cytometry, we also investigated the percentage of cells expressing the cell surface markers SSEA-3 and SSEA-4 in undifferentiated populations of patient and control iPS cell lines. No differences were observed in the percentage of cells expressing each marker between patient and control cell lines (Fig. 2E). Additionally, we analyzed genomic DNA from each iPS cell line for chromosomal integrity using a single nucleotide polymorphism (SNP) array (Supplemental Table 1). Finally, we generated embryoid bodies (EBs) from both patient and control derived iPS cell lines and assessed their ability to differentiate into all 3 germ layers. EBs spontaneously differentiated into cells from endoderm, ectoderm and mesoderm, as evidenced by immunofluorescence staining for alpha-fetoprotein (AFP), β-tubulin III and muscle actin (Fig. 2F).

3.3. Morphological characterization of patient and control derived cardiomyocytes

We induced cardiac differentiation of iPS cells and obtained cardiomyocytes (iPS-CM) which were aggregated in the form of beating bodies, and contracted spontaneously (Supplemental Videos 1 and 2). To compare the morphological properties of patient and control iPS-CM, we enzymatically and mechanically disaggregated 3–4 week old beating bodies for immunofluorescence staining. Disaggregation resulted in single as well as clusters of beating cardiomyocytes, with groups of connected cardiomyocytes exhibiting synchronized contraction. After 3–5 days of recovery, we fixed and stained cells for markers of the cardiac contractile apparatus (Fig. 3A). Control and patient cells isolated from beating bodies stained positive for alpha actinin, cardiac troponin I (cTnI) and cardiac troponin T (cTnT). Single cTnT staining exhibited the striated pattern of thin filaments while double staining for cTnI and alpha actinin resulted in alternating striations, staining thin filaments and *Z*-lines respectively.

We examined the structure of the contractile apparatus of beating bodies in more detail using transmission electron microscopy. In both patient and control iPS-CM, myofibrils varied in size with some consisting of a single sarcomere. Some cells contained a greater number of myofibrils with increased organization, exhibiting some alignment of *Z*-lines between adjacent myofibrils (Fig. 3B, left). At high magnification, we observed sarcomeres with I-bands and A-bands in addition to Z-lines (Fig. 3B, right).

3.4. Electrophysiological characterization of patient and control derived cardiomyocytes

We first studied the sodium current properties of patient and control iPS-CM generated using an embryoid body based differentiation protocol. Cardiomyocytes were derived from two different patient iPS cell clones. Two separate differentiations for each clone were used for our

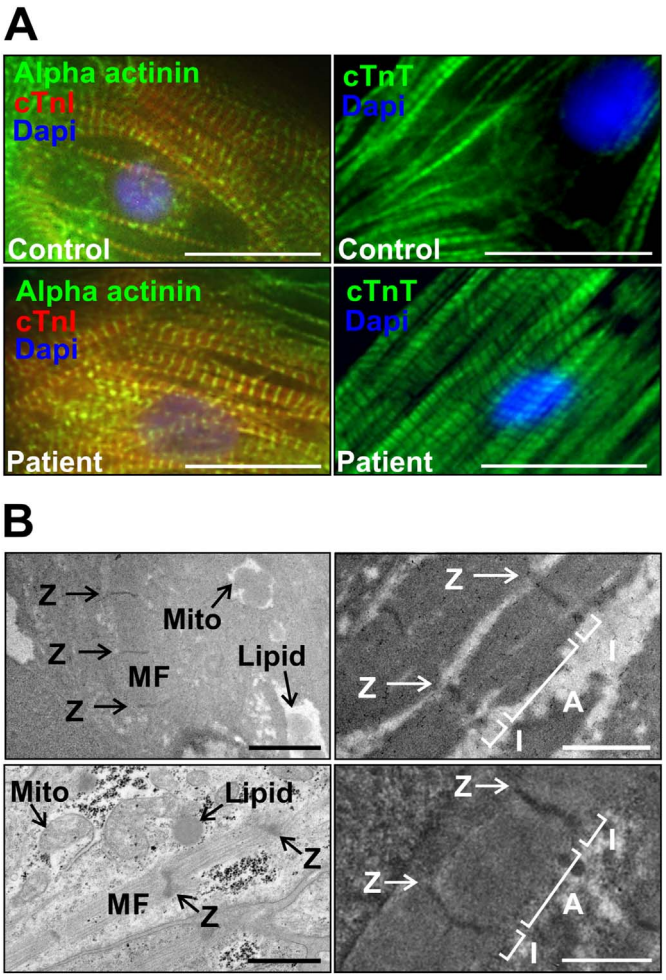

Fig. 3. Control and patient-specific iPS-CM show typical patterns for cardiac markers. (A) Control (top panels) and patient (bottom panels) iPS-CM stained positive for alpha actinin and cardiac Troponin I (left), and cardiac Troponin T (right), showing intact myofibrils. Nuclei were counterstained with DAPI (blue). Figure shows representative merged images. Scale bars represent 20 μm. (B) Control (top panels) and patient (bottom panels) iPS-CM showed mitochondria (Mito) and lipid deposits (Lipid) as well as myofibrils (MF) of varying width and length (left). We also observed sarcomeres with I bands (I) and A bands (A) in addition to Z lines (Z) (right). Scale bars represent 1 μm.

study. All these iPS-CM were characterized independently. The sodium current properties of each of the lines were compared to the results obtained from cardiomyocytes derived from one control iPS cell line. Since the results obtained for the two differentiations per clone and for the two patient iPS-CM clones were very similar, data was pooled. Whole cell current recordings showed a loss of function of the sodium channel current in patient-derived compared to control-derived cardiomyocytes. Representative examples of I_{Na} traces for patient and control cardiomyocytes at varying potentials are shown in Fig. 4A. Peak I_{Na} density was reduced by 45.5% in patient-derived compared to control-derived cardiomyocytes ($p < 0.05$, Fig. 4B, Table 1). In addition, voltage-activation data fit to a Boltzmann equation revealed a positive 7.42 mV shift of the $V_{1/2}$ in patient respect to control cells, without significant changes in the slope factor (Fig. 4C, Table 1). Steady-state voltage dependence of inactivation data fit to a Boltzmann equation evidenced a negative shift of 8.51 mV of the $V_{1/2}$ in patient respect to control cells, and no significant changes in the slope factor (Fig. 4C, Table 1). Analysis of recovery from inactivation time course is illustrated in Fig. 4D. Data was fitted with a bi-exponential function and revealed a faster recovery in the patient cells (Table 1).

In a second set of experiments, we studied the sodium current properties of patient and control iPS-CM generated using a monolayer-based differentiation protocol. For these experiments, we used one of the patient iPS cell lines and an additional healthy control iPS cell line (Supplemental Videos 3 and 4). Whole cell current recordings showed a loss of function of the sodium channel current in patient-derived compared to control-derived cardiomyocytes. Examples of I_{Na} traces are depicted in Supplemental Fig. 1A. Analysis of the data revealed a reduction of 33.12% in peak current density in the patient-derived compared to control-derived iPS-CM ($p < 0.05$; Supplemental Fig. 1B and Table 1). It is worth noting that this analysis shows an underestimation of the current reduction since 6 out of 17 control cells displayed currents too large to allow proper voltage control in our already low sodium recording conditions. Furthermore, we observed a positive 7.53 mV shift in the activation $V_{1/2}$, and a negative 5.89 mV shift in the steady-state inactivation $V_{1/2}$ in patient respect to control cells ($p < 0.001$ and $p < 0.01$, respectively; Supplemental Fig. 1C and Table 1). As in the first set of experiments, we observed a faster recovery from inactivation in the patient iPS-CM respect to control ($p < 0.05$, Supplemental Fig. 1D and Table 1).

3.5. Electrophysiology and cell surface protein biotinylation in tsA201 cells

It is worth noting that the available studies of $Na_v1.5$_p.R367H had been performed in a homozygous state for either the WT or the mutant gene (WT/WT or R367H/R367H). They showed a total loss of I_{Na} when only mutant channels were expressed, both in HEK293 cells and in *Xenopus* oocytes. Conversely, our patient carried the mutant channel in a heterozygous state (WT/R367H), and our results in iPS-CM showed differences in the biophysical properties of the current obtained in the patient compared to the control cells. This prompted us to study the biophysical properties of the sodium current in tsA201 cells transiently expressing sodium channels in heterozygous conditions. In contrast with the iPS-CM, in this setting the only difference between cells would be the point mutation of interest.

We transfected tsA201 cells with either the vector encoding $Na_v1.5$_WT (homozygous WT cells), the vector encoding $Na_v1.5$_R367H (homozygous R367H cells) or both vectors (heterozygous WT/R367H cells). We performed the electrophysiological recordings on isolated cells 48 h after transfection using whole cell patch-clamping and normal sodium bath solution. Representative examples of I_{Na} traces for the 3 conditions are shown in Fig. 5A. Recordings performed in cells transfected with only $Na_v1.5$_R367H revealed a complete loss of current (Fig. 5A, lower panel). Peak I_{Na} density was significantly reduced by 49.8% in heterozygous WT/R367H cells with respect to homozygous WT/WT cells (Fig. 5B). No further changes in $V_{1/2}$ were observed after data fitting in either activation or steady-state inactivation (Fig. 5C, Table 2) or in the recovery from inactivation time course (Fig. 5D, Table 2).

Previous immunofluorescence assays of $Na_v1.5$_p.R367H expressed in HEK293 cells had shown that the mutant channels could reach the plasma membrane [14]. To quantify whether the WT and mutant channels localized at the cell surface in similar amounts, we performed protein biotinylation assays in tsA201 cells. Fig. 5E and F show that the cell surface $Na_v1.5$ expression was similar in homozygous $Na_v1.5$_WT cells, homozygous $Na_v1.5$_R367H cells and heterozygous WT/R367H cells. Therefore, the p.R367H $Na_v1.5$ channels could traffic efficiently to the plasma membrane, and did not interfere in WT channel trafficking.

4. Discussion

Sodium channel current loss of function has been long and widely accepted as a hallmark of Brugada syndrome. Still, most of the evidence comes from heterologous expression studies. To date, only two studies have shown evidence for the association of a sodium channel mutation with either Brugada syndrome or overlapped LQT3/Brugada syndrome in iPS-CM [8,9]. However, these studies only show a reduction in

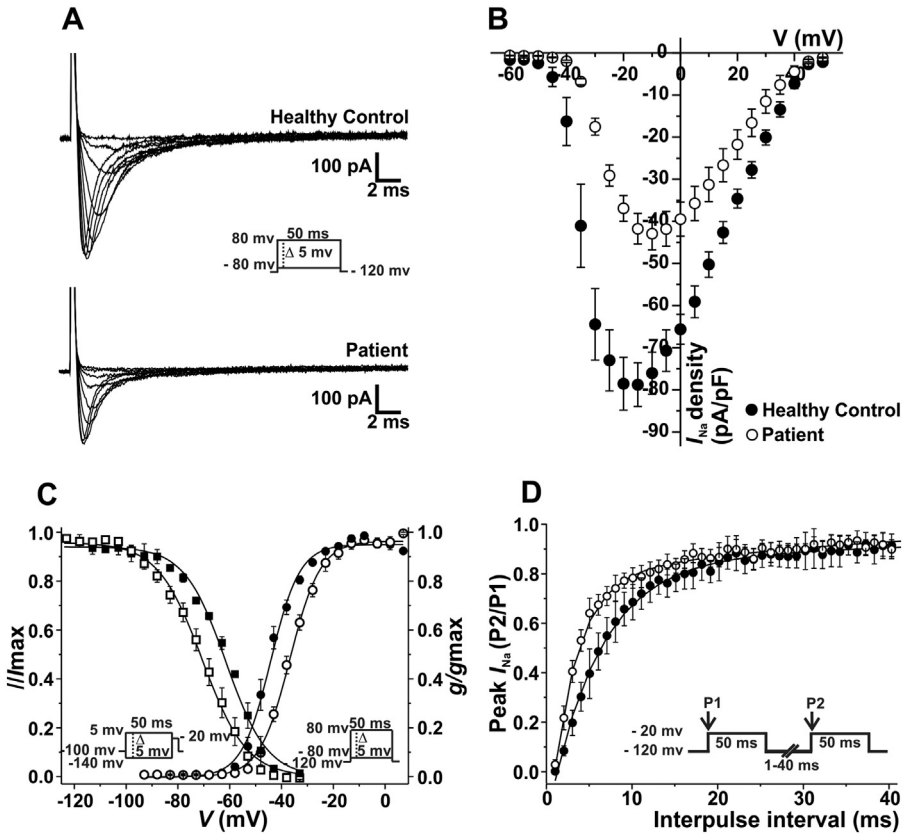

Fig. 4. Patient-specific iPS-CM display altered I_{Na} properties. Filled symbols are used to depict data for healthy control iPS-CM and open symbols represent values for patient-specific cardiomyocytes. Values are expressed as mean ± SEM. (A) Representative whole cell sodium current traces recorded from control and patient-specific cells. Currents were elicited by depolarizing potentials as shown in the inset. Traces for pulses from − 50 mV to − 15 mV are shown. (B) Current-voltage (I–V) relationship. I_{Na} amplitude was normalized to the cell capacitance to obtain current density (I_{Na} density) values. Experimental points represent the peak-amplitude of I_{Na} density at each given voltage. (C) I_{Na} voltage-dependence of activation and steady-state inactivation for control and patient cells. Conductance values for the activation curve were obtained from the peak current values taken from the I–V relationship. Symbols represent experimental data plotted against the given depolarizing voltage values. Steady-state inactivation protocol is shown in the inset on the left. Symbols represent experimental data plotted against pre-conditioning pulse values. Solid lines represent the Boltzmann fit of the experimental points. (D) Recovery from inactivation properties were studied by applying the double pulse protocol shown in the inset. A 50 ms depolarizing pulse to − 20 mV (P1) was followed by a hyperpolarizing pulse to − 120 mV of increasing duration (1–40 ms), that preceded a test pulse to − 20 mV (P2). The P2/P1 ratio values plotted against the recovery interval times were fitted to bi-exponential functions (solid lines).

Table 1
Biophysical parameters of WT and mutant channels in iPS-CM.

Parameter	Beating bodies		Monolayer	
	Healthy control iPS-CM	Patient iPS-CM	Healthy control iPS-CM	Patient iPS-CM
Peak I_{Na}				
pA/pF	− 78.77 ± 5.16	− 42.93 ± 3.86***	− 45.62 ± 5.37	− 30.51 ± 3.09*
n	3	7	11	13
Activation				
$V_{1/2}$ (mV)	− 44.15 ± 0.37	− 36.73 ± 0.32***	− 32.96 ± 0.79	− 25.44 ± 0.78***
k	5.57 ± 0.33	5.86 ± 0.28	3.94 ± 0.14	5.58 ± 0.26***
n	3	7	11	13
Steady-state inactivation				
$V_{1/2}$ (mV)	− 61.64 ± 0.77	− 70.15 ± 2.76*	− 48.80 ± 0.79	− 54.69 ± 1.21**
k	8.94 ± 1.54	8.70 ± 0.57	6.70 ± 0.33	9.59 ± 0.24***
n	3	7	8	10
Recovery from inactivation				
τ (ms)	τf: 5.85 ± 1.01	τf: 2.89 ± 0.35**	τf: 2.58 ± 0.31	τf: 1.68 ± 0.18*
	τs: 40.38 ± 4.95	τs: 34.45 ± 14.45	τs: 46.17 ± 7.01	τs: 20.12 ± 6.76*
n	3	6	5	5

Activation and steady-state inactivation parameters were calculated by data fitting to Boltzmann functions (see Materials and methods). $V_{1/2}$ is the voltage for half-maximal activation or steady-state inactivation, *k* is the slope factor and *n* the number of cells. Recovery from inactivation data was fitted to a bi-exponential function (see Materials and methods) to obtain the fast and slow time constants (τf and τs, respectively). Values are expressed as mean ± SEM.

* $p < 0.05$.
** $p < 0.01$.
*** $p < 0.001$.

sodium current density in patient iPS-CM compared to the control iPS-CM. Thus, our present study is the first to show the loss of sodium channel function by a complete characterization of the sodium current properties in native cells from a BrS patient who carries a mutation in *SCN5A*. Although expected, it is not trivial to show in native cells that a mutation that causes total loss of function of the current provokes a reduction of the total current to 50%. In fact, we identified in the iPS-CM further pro-arrhythmic changes in channel function that could not be detected using conventional heterologous expression systems. It is to note that a comparison of the effects of *SCN5A* mutations on sodium current properties in both model systems had never been performed before for Brugada syndrome.

We successfully generated iPS cells through reprogramming of dermal fibroblasts from a Brugada syndrome patient and an age and sex-matched healthy volunteer. No differences were observed between patient and control iPS cell lines in terms of colony morphology,

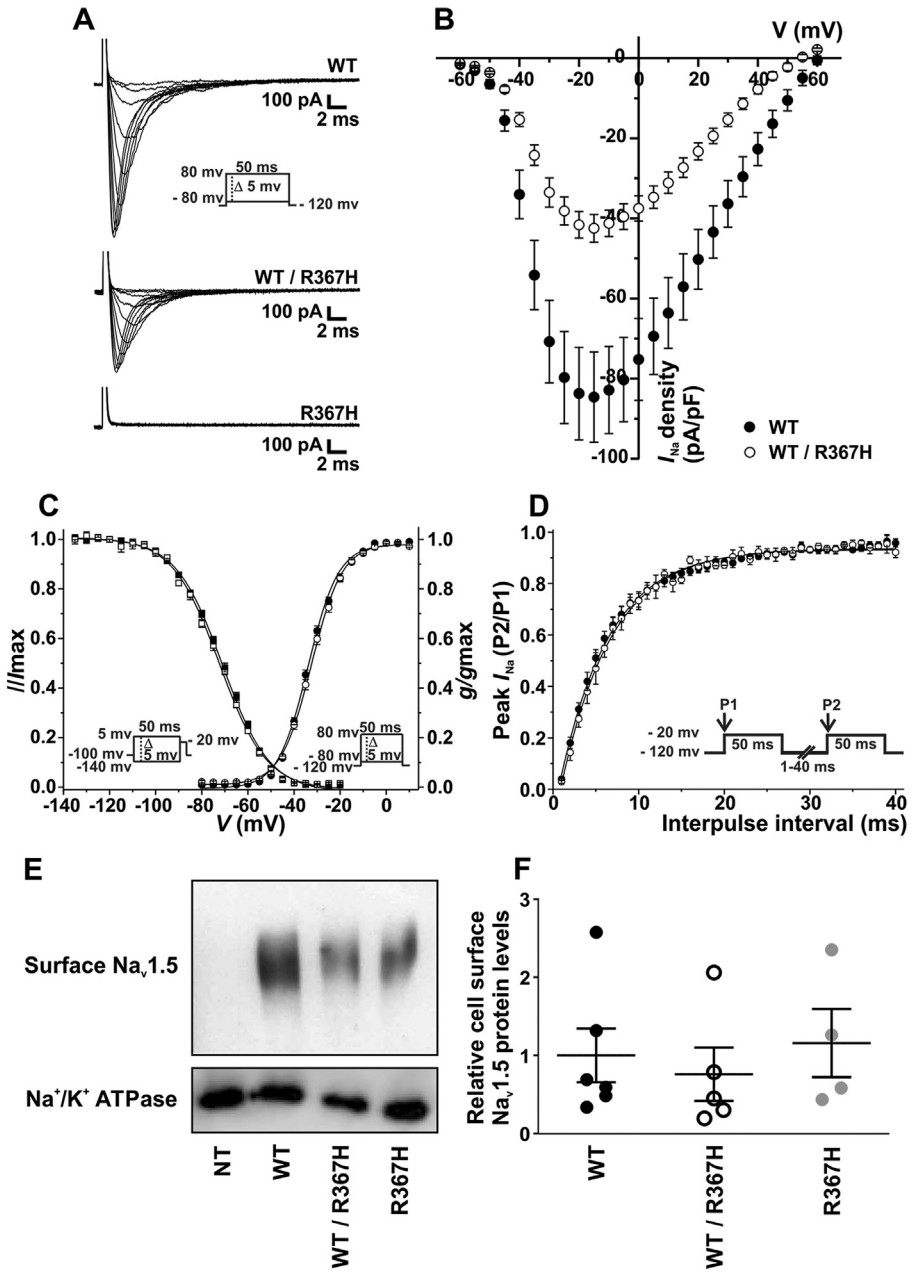

Fig. 5. $Na_v1.5\_R367H$ markedly decreases peak I_{Na}. (A) Representative whole cell sodium current traces recorded from WT, WT/R367H and R367H cells. Currents were elicited by depolarizing potentials as shown in the inset. Traces for pulses from − 60 mV to − 5 mV are shown. (B–D) Filled symbols are used to depict data for WT cells, and open symbols represent values for WT/R367H cells. Values are expressed as mean ± SEM. (B) Current-voltage (I–V) relationship. I_{Na} amplitude was normalized to the cell capacitance to obtain current density (I_{Na} density) values. Experimental points represent the peak-amplitude of I_{Na} density at each given voltage. (C) I_{Na} voltage-dependence of activation and steady-state inactivation for WT and WT/R367H cells. Conductance values for the activation curve were obtained from the peak current values taken from the I–V relationship. Symbols represent experimental data plotted against the given depolarizing voltage values. Steady-state inactivation protocol is shown in the inset on the left. Symbols represent experimental data plotted against preconditioning pulse values. Solid lines represent the Boltzmann fit of the experimental points. (D) Recovery from inactivation properties were studied by applying the double pulse protocol shown in the inset. A 50 ms depolarizing pulse to − 20 mV (P1) was followed by a hyperpolarizing pulse to − 120 mV of increasing duration (1–40 ms), that preceded a test pulse to − 20 mV (P2). The P2/P1 ratio values plotted against the recovery interval times were fitted to mono-exponential functions (solid lines). (E) Representative image of western blot detection of $Na_v1.5$ and Na^+/K^+ ATPase proteins performed after cell surface biotinylation of non-transfected cells (NT), cells transfected only with the vector encoding $Na_v1.5\_WT$ (WT), with the vectors encoding $Na_v1.5\_WT$ and $Na_v1.5\_R367H$ (WT/R367H) and only with the vector encoding $Na_v1.5\_R367H$ (R367H). (F) Scatter plot showing the relative surface $Na_v1.5$ protein expression. Intensity values were calculated as described in Methods and normalized relative protein expression was plotted for each of the replicates (dots). Lines represent means ± SEM.

expression of pluripotency transcription factors and proteins, or their ability to differentiate into the three germ layers. As anticipated, the only difference was the presence of the patient's mutation (*SCN5A*_c.1100G > A) in the patient-specific iPS cell lines and its absence in those obtained from the healthy volunteer.

Comparison of ultrastructure and staining for markers of the cardiac contractile apparatus did not show any obvious differences between cardiomyocytes derived from patient-specific and healthy control pluripotent stem cells. Importantly, the analysis of electrophysiological recordings revealed a 33.1–45.5% reduction of peak I_{Na} density in patient-derived compared to healthy control-derived cardiomyocytes. This decrease represents a loss of function of the sodium channel. Previous findings had shown a complete loss of function of homozygous $Na_v1.5\_R367H$ channels [10–13]. In heterozygous conditions, a reduction of I_{Na} to 50%, most likely originated only from the expression of the WT allele, would be expected. This is consistent with reduced peak I_{Na} density that we observed in the patient iPS-CM. Surprisingly, our iPS-CM model showed additional changes in other electrophysiological properties. We observed a positive shift in the voltage-dependence of activation and a negative shift in the voltage-dependence of steady-state inactivation in the patient-specific cardiomyocytes. These voltage-dependence changes further contribute to the loss of function of the sodium channel. We also detected a faster recovery from channel inactivation in the patient iPS-CM. This acceleration in channel recovery has been proposed to contribute to the generation of arrhythmias in Brugada syndrome patients [21]. Importantly, we observed similar changes in sodium current properties when comparing patient and control iPS-CM generated with two distinct differentiation protocols. Although the differences in the current between patient and control iPS-CM were qualitatively the same in both experimental sets, the magnitude of the effects was different. This variability is expected considering that iPS-CM were obtained by different protocols. Moreover, the control iPS-CM used in both protocols were from two non-related healthy individuals. The results obtained support the idea that I) the SNV under study has an effect on sodium current properties; and II) the individual-specific genetic background could modulate the magnitude of this

Table 2
Biophysical parameters of WT and mutant channels in tsA201 cells.

Parameter	WT tsA201 cells	WT/R367H tsA201 cells
Peak I_{Na}		
pA/pF	− 84.62 ± 11.24	− 42.48 ± 3.46**
n	11	10
Activation		
$V_{1/2}$ (mV)	− 33.91 ± 0.20	− 32.42 ± 0.22
k	6.54 ± 0.18	6.63 ± 0.20
n	11	10
Steady-state inactivation		
$V_{1/2}$ (mV)	− 71.03 ± 0.25	− 72.36 ± 0.32
k	10.17 ± 0.23	10.18 ± 0.29
n	11	6
Recovery from inactivation		
τ (ms)	5.80 ± 0.17	5.93 ± 0.23
n	6	4

Activation and steady-state inactivation parameters were calculated by data fitting to Boltzmann functions (see Materials and methods). $V_{1/2}$ is the voltage for half-maximal activation or steady-state inactivation, *k* is the slope factor and *n* the number of cells. Recovery from inactivation data was fitted to a mono-exponential function to obtain the time constant τ. Values are expressed as mean ± SEM.

** $p < 0.01$.

effect.

In support to our experimental data, we provide a comparison of the I_{Na} parameters reported here with those previously published for embryonic stem cell-derived cardiomyocytes (ES-CM), iPS-CM and native cardiomyocytes (Table 3). It is worth noting that the voltage for I_{Na} half-maximal activation that we recorded in our control cells is similar to that reported for native human cardiomyocyte preparations [22–27] (Table 3). Our value for EB-differentiated cardiomyocytes was even closer to that for native cells than that of other human iPS [28–30] and ES [31,32] cell derived cardiomyocytes. Regarding half-maximal steady-state inactivation voltage, the value reported for native preparations is clearly more hyperpolarized (by approx. 19 mV) than the one recorded in ES-CM, and this difference increases up to 33 mV when compared with that for iPS-CM. However, the values obtained in this study are in line with those reported for other iPS-CM (Table 3).

Table 3
Comparison of I_{Na} voltage-dependent properties.

	$V_{1/2}$ activation (mV)	$V_{1/2}$ steady-state inactivation(mV)
This study		
EB-based differentiation	− 44.15 ± 0.37 (*n* = 3)	− 61.48 ± 0.5 (*n* = 3)
Monolayer-based differentiation	− 32.96 ± 0.79 (*n* = 11)	− 48.80 ± 0.79 (*n* = 8)
iPS-CM		
Ma et al. [28]	− 34.1 (*n* = 5)	− 72.1 (*n* = 5)
Ma et al. [29]	− 39.68 ± 1.96 (*n* = 8)	− 44.63 ± 5.77 (*n* = 8)
Terrenoire et al. [30]	− 25 ± 0.3 (*n* = 3)	− 70.3 ± 1.7 (*n* = 3)
Terrenoire et al. [30]		− 68.9 ± 0.9 (*n* = 6)
ES-CM		
Satin et al. [31]	− 30 (*n* = 21)	− 72.6 ± 0.7 (*n* = 19)
Jonsson et al. [32]	− 34 (*n* = 7)	− 78 (*n* = 7)
Native cardiomyocytes		
Sakakibara et al. [23]	− 38.9 ± 0.9 (*n* = 46)	− 95.8 ± 0.9 (*n* = 46)
Sakakibara et al. [27]	− 42.3 ± 1.7 (*n* = 12)	− 99.8 ± 2.1 (*n* = 12)
Sakakibara et al. [27]	− 43.8 ± 0.2 (*n* = 10)	− 94.5 ± 2.3 (*n* = 10)
Feng et al. [26]	− 38.6 ± 2.9 (*n* = 6)	− 95.1 ± 5.4 (*n* = 6)
Valdivia et al. [24]	− 51 ± 1.0 (*n* = 11)	− 102 ± 16 (*n* = 3)
Valdivia et al. [24]	− 50 ± 1.1 (*n* = 17)	− 88 ± 1.9 (*n* = 10)
Barajas-Martínez et al. [25]	~ − 52	− 90.1 ± 0.9 (*n* = 3)
Jia et al. [22]		− 93 (*n* = 5)

The table shows the voltage for half-maximal activation and inactivation for control cells in each category. Values are expressed as mean ± SD or SEM, as reported in each original study (if available). The number of cells characterized in each work is provided (*n*).

Our cell surface protein biotinylation studies in tsA201 cells demonstrate that both WT and mutant channels reach the cell surface to a similar extent when $Na_v1.5$_R367H is expressed either in heterozygosis or homozygosis. Thus, the corresponding partial or total I_{Na} reduction would result from a mutant non-functional channel rather than by a trafficking defect, in agreement with previous studies [14]. Due to the limited amount of tissue available from iPS-CM, we could not perform biotinylation studies with these cells. However, based on our results from tsA201 cells, a trafficking defect in iPS-CM caused by the mutation would be unlikely. Consequently, these results argue against a negative dominant effect of p.R367H as it has been shown for other mutations in $Na_v1.5$ [33,34].

Nevertheless, a functional interaction between sodium channel alpha subunits could account for the differences in voltage-dependent and kinetic properties of the sodium current that we observed between patient and control iPS-CM. Indeed, recent structural studies of the $Na_v1.5$ channel have shown evidence for the formation of asymmetric α-subunit dimers [35]. The authors propose that the dimerization of the α subunits would be mediated through the binding of calmodulin to their C-terminus. The mutation studied in the present study (p.R367H) is far from the C-terminus of the sodium channel, and thus would not be expected to interfere with dimerization. However, if as proposed, functional Na_v channels do exist in oligomeric states involving at least two α subunits, functional interactions between WT and mutant α subunits could explain the kinetic and voltage dependent differences in patient-specific iPS-CM compared to control. We did not observe such differences in current properties in tsA201 cells. This might be due to unbalanced amounts of endogenous calmodulin or other sodium channel modulatory molecules, and the overexpressed $Na_v1.5$ in tsA201 cells. Conversely, iPS-CM are likely to possess the molecular machinery to allow $Na_v1.5$ oligomerization. Thus, the formation of heterodimers (WT/R367H) could account for the differences in I_{Na} observed between the patient and control iPS-CM.

Overall, the two cellular models studied in this work present important differences. It should be considered that the experimental conditions for tsA201 cells (homozygous WT/WT vs. heterozygous WT/mutant) only differ in the transfected gene. On the other hand, the patient and the control iPS-CM are likely to carry variations in their genetic background in addition to the patient's mutation. Some of these variations could affect cardiac-specific proteins (e.g. channel auxiliary subunits) which are not expressed in tsA201 cells. These variations, either common or rare, could influence the sodium current's biophysical properties. Altogether, our work points to these differences as a possible explanation of why electrophysiological changes other than reduced peak I_{Na} were evident only when analyzing iPS-CM but not in the heterologous tsA201 cell model.

Our results suggest that the patient-specific genetic background could be a critical determinant of the phenotypical manifestation of Brugada syndrome. Finally, our work highlights the need of assessing the pathophysiological mechanisms of sodium channel mutations in a cardiac- and patient-specific model.

5. Study limitations

Our results illustrate the ability of patient-specific iPS cell technology to model the abnormal functional phenotype of Brugada syndrome. Nevertheless, an issue still remains, which is the maturity of the obtained iPS-CM. Although cardiomyocytes derived from iPS cells usually represent a mixture of cells with different degrees of maturity, it has been demonstrated that human iPS-CM have all major cardiac ionic

currents, including I_{Na}, $I_{Ca\text{-}L}$, I_f, I_{to}, I_{K1}, I_{Kr}, I_{Ks} and $I_{K,ATP}$ [28,36,37] and would thus be suitable for examining ion channel function in a patient-specific context. In this sense, we have shown that the cardiomyocytes obtained from our patient and control exhibit typical cardiac markers and have functional cardiac sodium channels. Therefore, our results support the accepted current idea that the relative immaturity of iPS-CM does not prevent their use as an accurate system to model channelopathies affecting $Na_v1.5$. Nevertheless, due to this limitation, we focused our studies on the sodium current since this is less subject to cell variability than action potentials.

It is important to acknowledge that we cannot generalize our results to other sodium channel mutations. Thus, at the moment our conclusions should be limited to the specific variant studied in this work. Nonetheless, we believe that our findings represent important evidence on how the cellular environment may contribute to the phenotypical expression of a sodium channel mutation.

6. Conclusions

Cardiomyocytes derived from iPS cells from a Brugada syndrome patient with a mutation in *SCN5A* recapitulate the loss of function of the sodium channel current associated with this syndrome, including pro-arrhythmic changes in channel function that could only be detected using iPS-CM and not in conventional heterologous expression systems. We believe that our findings underscore the extra value that the use of patient-specific iPS-CM confers to mutation studies in BrS. Therefore, we expect that our work will contribute to establish iPS-CM as an adequate cell model for the investigation of BrS.

Supplementary data to this article can be found online at https://doi.org/10.1016/j.yjmcc.2017.10.002.

Disclosures

None.

Acknowledgements

The authors thank Dr. Ariel Escobar for his critical revision and valuable comments on the manuscript. This work was supported by the British Heart Foundation through an Intermediate Clinical Research Fellowship [grant number FS/10/024/28266], by a UK Cardiovascular Regenerative Medicine Centre Award [grant number RM/17/3/33381], by Obra social “la Caixa”, by Centro Nacional de Investigaciones Cardiovasculares [grant number CNIC-03-2008], by Instituto de Salud Carlos III [grant number FIS-PI08/1800 and Fondo Europeo de Desarrollo Regional] and by La Marató de TV3 [grant number 20153910]. The CIBERCV is an initiative of the Instituto de Salud Carlos III, Spanish Ministry of Economy and Competitiveness. FS was funded by the College of Medicine & Veterinary Medicine, University of Edinburgh, ES was a Sara Borrell fellow, GJP and FSS are Serra Hunter fellows, and OTC was the recipient of IDIBAPS-Marie-Curie Biotrack postdoctoral fellowship. The funders had no role in study design, data collection and analysis, decision to publish, or preparation of the manuscript.

References

[1] C. Antzelevitch, P. Brugada, M. Borggrefe, J. Brugada, R. Brugada, D. Corrado, et al., Brugada syndrome: report of the second consensus conference, Heart Rhythm. 2 (2005) 429–440.
[2] P. Brugada, J. Brugada, Right bundle branch block, persistent ST segment elevation and sudden cardiac death: a distinct clinical and electrocardiographic syndrome. A multicenter report, J. Am. Coll. Cardiol. 20 (6) (1992) 1391.
[3] P. Brugada, R. Brugada, J. Brugada, P. Geelen, Use of the prophylactic implantable cardioverter defibrillator for patients with normal hearts, Am. J. Cardiol. 83 (1999) 98D–100D.
[4] J. Brugada, R. Brugada, P. Brugada, Pharmacological and device approach to therapy of inherited cardiac diseases associated with cardiac arrhythmias and sudden death, J. Electrocardiol. (33 Suppl) (2000) 41–47.
[5] J.B. Gourraud, J. Barc, A. Thollet, S. Le Scouarnec, H. Le Marec, J.J. Schott, et al., The Brugada syndrome: a rare arrhythmia disorder with complex inheritance, Front. Cardiovasc. Med. 3 (2016) 9.
[6] Q. Chen, G. Kirsch, D. Zhang, R. Brugada, J. Brugada, P. Brugada, et al., Genetic basis and molecular mechanism for idiopathic ventricular fibrillation, Nature 392 (1998) 293–296.
[7] P. Dell'Era, P. Benzoni, E. Crescini, M. Valle, E. Xia, A. Consiglio, et al., Cardiac disease modeling using induced pluripotent stem cell-derived human cardiomyocytes, World J. Stem Cells 7 (2015) 329–342.
[8] R.P. Davis, S. Casini, C.W. van den Berg, M. Hoekstra, C.A. Remme, C. Dambrot, et al., Cardiomyocytes derived from pluripotent stem cells recapitulate electrophysiological characteristics of an overlap syndrome of cardiac sodium channel disease, Circulation 125 (2012) 3079–3091.
[9] P. Liang, K. Sallam, H. Wu, Y. Li, I. Itzhaki, P. Garg, et al., Patient-specific and genome-edited induced pluripotent stem cell-derived cardiomyocytes elucidate single-cell phenotype of Brugada syndrome, J. Am. Coll. Cardiol. 68 (2016) 2086–2096.
[10] K. Hong, A. Berruezo-Sanchez, N. Poungvarin, A. Oliva, M. Vatta, J. Brugada, et al., Phenotypic characterization of a large European family with Brugada syndrome displaying a sudden unexpected death syndrome mutation in SCN5A, J. Cardiovasc. Electrophysiol. 15 (2004) 64–69.
[11] N. Takehara, N. Makita, J. Kawabe, N. Sato, Y. Kawamura, A. Kitabatake, et al., A cardiac sodium channel mutation identified in Brugada syndrome associated with atrial standstill, J. Intern. Med. 255 (2004) 137–142.
[12] K. Shinlapawittayatorn, L.A. Dudash, Du XX, L. Heller, S. Poelzing, E. Ficker, et al., A novel strategy using cardiac sodium channel polymorphic fragments to rescue trafficking-deficient SCN5A mutations, Circ. Cardiovasc. Genet. 4 (2011) 500–509.
[13] M. Vatta, R. Dumaine, G. Varghese, T.A. Richard, W. Shimizu, N. Aihara, et al., Genetic and biophysical basis of sudden unexplained nocturnal death syndrome (SUNDS), a disease allelic to Brugada syndrome, Hum. Mol. Genet. 11 (2002) 337–345.
[14] H. Watanabe, A. Nogami, K. Ohkubo, H. Kawata, Y. Hayashi, T. Ishikawa, et al., Electrocardiographic characteristics and SCN5A mutations in idiopathic ventricular fibrillation associated with early repolarization, Circ. Arrhythm. Electrophysiol. 4 (2011) 874–881.
[15] X. Xu, R. Graichen, S. Soo, T. Balakrishnan, S. Rahmat, S. Sieh, et al., Chemically defined medium supporting cardiomyocyte differentiation of human embryonic stem cells, Differentiation 76 (2008) 958–970.
[16] V.A. Maltsev, A.M. Wobus, J. Rohwedel, M. Bader, J. Hescheler, Cardiomyocytes differentiated in vitro from embryonic stem cells developmentally express cardiac-specific genes and ionic currents, Circ. Res. 75 (1994) 233–244.
[17] C.L. Mummery, D. Ward, R. Passier, Differentiation of human embryonic stem cells to cardiomyocytes by coculture with endoderm in serum-free medium, Curr. Protoc. Stem Cell Biol. (2007) Chapter 1:Unit 1F.2.
[18] Y. Lin, K.L. Linask, B. Mallon, K. Johnson, M. Klein, J. Beers, et al., Heparin promotes cardiac differentiation of human pluripotent stem cells in chemically defined albumin-free medium, enabling consistent manufacture of cardiomyocytes, Stem Cells Transl. Med. 6 (2017) 527–538.
[19] A. Tarradas, E. Selga, P. Beltran-Alvarez, A. Perez-Serra, H. Riuro, F. Pico, et al., A novel missense mutation, I890T, in the pore region of cardiac sodium channel causes Brugada syndrome, PLoS One 8 (2013) e53220.
[20] O.P. Hamill, A. Marty, E. Neher, B. Sakmann, F.J. Sigworth, Improved patch-clamp techniques for high-resolution current recording from cells and cell-free membrane patches, Pflugers Arch. 391 (1981) 85–100.
[21] I. Gussak, C. Antzelevitch, P. Bjerregaard, J.A. Towbin, B.R. Chaitman, The Brugada syndrome: clinical, electrophysiologic and genetic aspects, J. Am. Coll. Cardiol. 33 (1999) 5–15.
[22] H. Jia, T. Furukawa, D.H. Singer, Y. Sakakibara, S. Eager, C. Backer, et al., Characteristics of lidocaine block of sodium channels in single human atrial cells, J. Pharmacol. Exp. Ther. 264 (1993) 1275–1284.
[23] Y. Sakakibara, J.A. Wasserstrom, T. Furukawa, H. Jia, C.E. Arentzen, R.S. Hartz, et al., Characterization of the sodium current in single human atrial myocytes, Circ. Res. 71 (1992) 535–546.
[24] C.R. Valdivia, W.W. Chu, J. Pu, J.D. Foell, R.A. Haworth, M.R. Wolff, et al., Increased late sodium current in myocytes from a canine heart failure model and from failing human heart, J. Mol. Cell. Cardiol. 38 (2005) 475–483.
[25] H. Barajas-Martínez, D. Hu, R.J. Goodrow, F. Joyce, C. Antzelevitch, Electrophysiologic characteristics and pharmacologic response of human cardiomyocytes isolated from a patient with hypertrophic cardiomyopathy, Pacing Clin. Electrophysiol. 36 (2013) 1512–1515.
[26] J. Feng, G.R. Li, B. Fermini, S. Nattel, Properties of sodium and potassium currents of cultured adult human atrial myocytes, Am. J. Phys. 270 (1996) H1676–86.
[27] Y. Sakakibara, T. Furukawa, D.H. Singer, H. Jia, C.L. Backer, C.E. Arentzen, et al., Sodium current in isolated human ventricular myocytes, Am. J. Phys. 265 (1993) H1301–9.
[28] J. Ma, L. Guo, S.J. Fiene, B.D. Anson, J.A. Thomson, T.J. Kamp, et al., High purity human-induced pluripotent stem cell-derived cardiomyocytes: electrophysiological properties of action potentials and ionic currents, Am. J. Physiol. Heart Circ. Physiol. 301 (2011) H2006–17.
[29] D. Ma, H. Wei, Y. Zhao, J. Lu, G. Li, N.B. Sahib, et al., Modeling type 3 long QT syndrome with cardiomyocytes derived from patient-specific induced pluripotent stem cells, Int. J. Cardiol. 168 (2013) 5277–5286.
[30] C. Terrenoire, K. Wang, K.W. Tung, W.K. Chung, R.H. Pass, Lu JT, et al., Induced pluripotent stem cells used to reveal drug actions in a long QT syndrome family with complex genetics, J. Gen. Physiol. 141 (2013) 61–72.

[31] J. Satin, I. Kehat, O. Caspi, I. Huber, G. Arbel, I. Itzhaki, et al., Mechanism of spontaneous excitability in human embryonic stem cell derived cardiomyocytes, J. Physiol. 559 (2004) 479–496.
[32] M.K. Jonsson, M.A. Vos, G.R. Mirams, G. Duker, P. Sartipy, T.P. de Boer, et al., Application of human stem cell-derived cardiomyocytes in safety pharmacology requires caution beyond hERG, J. Mol. Cell. Cardiol. 52 (2012) 998–1008.
[33] J. Clatot, A. Ziyadeh-Isleem, S. Maugenre, I. Denjoy, H. Liu, G. Dilanian, et al., Dominant-negative effect of SCN5A N-terminal mutations through the interaction of Na(v)1.5 alpha-subunits, Cardiovasc. Res. 96 (2012) 53–63.
[34] M. Hoshi, Du XX, K. Shinlapawittayatorn, H. Liu, S. Chai, X. Wan, et al., Brugada syndrome disease phenotype explained in apparently benign sodium channel mutations, Circ. Cardiovasc. Genet. 7 (2014) 123–131.
[35] S.B. Gabelli, A. Boto, V.H. Kuhns, M.A. Bianchet, F. Farinelli, S. Aripirala, et al., Regulation of the NaV1.5 cytoplasmic domain by calmodulin, Nat. Commun. 5 (2014) 5126.
[36] M. Honda, J. Kiyokawa, M. Tabo, T. Inoue, Electrophysiological characterization of cardiomyocytes derived from human induced pluripotent stem cells, J. Pharmacol. Sci. 117 (2011) 149–159.
[37] D.K. Lieu, Fu JD, N. Chiamvimonvat, K.C. Tung, G.P. McNerney, T. Huser, et al., Mechanism-based facilitated maturation of human pluripotent stem cell-derived cardiomyocytes, Circ. Arrhythm. Electrophysiol. 6 (2013) 191–201.